European Cells and Materials Vol.49 2025 (pages 1–16) DOI: 10.22203/eCM.v049a01 ISSN 1473-2262

Original Article

EVALUATION OF HOLOTHURIAN OSSICLES AS A BIOLOGICAL BIOMATERIAL FOR MANDIBULAR BONE REGENERATION

O. Ortiz-Arrabal[1,2,§], E. Bullejos-Martínez[3,4,§], J. Chato-Astrain[1,2], V. Carriel[1,2], A. Martínez-Plaza[5,6], M.A. Martín-Piedra[1,2], I. Garzón[1,2], R. Fernandez-Valades[1,2,5], A. España-López[5,7,*], I.Á. Rodríguez[1,8,*] and M. Alaminos[1,2]

[1]Tissue Engineering Group, Department of Histology, School of Medicine, University of Granada, 18016 Granada, Spain
[2]Biomedical Research Institute (Instituto de Investigación Biosanitaria ibs.GRANADA), 18012 Granada, Spain
[3]University Hospital Foundation Jiménez Díaz, 28040 Madrid, Spain
[4]Doctoral Program in Clinical Medicine and Public Health, University of Granada, 18071 Granada, Spain
[5]Craniofacial Malformations and Cleft Lip and Palate Management Unit, University Hospital Virgen de las Nieves, 18014 Granada, Spain
[6]Division of Oral y Maxillofacial Surgery, University Hospital Virgen de las Nieves, 18014 Granada, Spain
[7]Department of Stomatology, School of Dentistry, University of Granada, 18071 Granada, Spain
[8]Department of Histology B, Faculty of Dentistry, National University of Cordoba, X5000HUA Cordoba, Argentina
[§]These authors contributed equally.

Abstract

Purpose: In the present study, we used holothurian ossicles (HOLO) extracted from sea cucumbers (holothurians) as novel biomaterials potentially useful in mandibular bone regeneration. **Methods:** HOLO particles were evaluated *ex vivo* and *in vivo* to determine biocompatibility and effectiveness in an animal model of bone defect. **Results:** First, *ex vivo* analyses found that HOLO were highly biocompatible when used with human cell cultures, as determined by LIVE/DEAD and DNA quantification assays, especially after 48 and 72 h of incubation. In contrast to control bone mineral particles (BP), cells cultured with HOLO tended to attach to these particles rather than to the culture surface, suggesting that the surface of HOLO could favor cell adhesion. *In vivo* analyses in Wistar rats showed that animals in which HOLO were grafted subcutaneously were devoid from any detectable side effects both at the systemic and local levels, and HOLO triggered a pro-regenerative M2-type macrophage response. When HOLO were applied in a model of mandibular bone defect, we found a positive effect of these particles as compared to negative controls, with a significant reduction of the size of the bone defect (3.36 ± 0.84 mm in HOLO vs. 9.16 ± 4.18 mm in controls) as determined by computed tomography (CT). Histologically, HOLO were associated to some ossification spots showing positive staining for toluidine blue, suggesting a process of osteoid formation, and an increased expression of osteonectin and osteocalcin, which were comparable or higher than control bone. **Conclusions:** These results suggest that HOLO could be safely used to induce mandible bone regeneration, and the use of these particles is associated to an increased bone regeneration process. Future studies should determine the clinical usefulness of these novel particles used in regenerative medicine.

Keywords: Bone regeneration, holothurian particles, grafts, tissue engineering.

***Address for correspondence**: A. España-López, Craniofacial Malformations and Cleft Lip and Palate Management Unit, University Hospital Virgen de las Nieves, 18014 Granada, Spain; Department of Stomatology, School of Dentistry, University of Granada, 18071 Granada, Spain. Email: ajep@ugr.es; I.Á. Rodríguez, Tissue Engineering Group, Department of Histology, School of Medicine, University of Granada, 18016 Granada, Spain; Department of Histology B, Faculty of Dentistry, National University of Cordoba, X5000HUA Cordoba, Argentina. Email: ismael.rodriguez@unc.edu.ar.

Introduction

Human oral and maxillofacial tissues can be affected by numerous congenital and acquired diseases that include tumors, trauma, infections, radionecrosis, and many other conditions [1]. In severe cases, these pathologies may lead to bone loss that is very difficult to treat and represents a therapeutic challenge [2,3].

Oral and maxillofacial bone loss can be treated using guided bone regeneration techniques [4]. However, extensive bone loss often requires the use of bone grafts, with autologous bone being considered as the reference technique in bone regeneration [5]. When autologous bone grafts are not an option, bone defects can be treated using different types of biomaterials, including synthetic particles [6], hydrogels [7,8], three-dimensional (3D)-printed materials [9] and other types of materials. One of the most commonly used biomaterials in cases when a bone defect must be surgically filled is bovine bone mineral particles (BP), which can be considered as a gold-standard filling treatment [10,11]. In most patients, the outcomes of the treatment based on biomaterial grafting are partially positive, with limited formation of regenerated bone [12]. However, the ideal biomaterial has not been developed to the date, and novel products able to facilitate an efficient regeneration of the oral and maxillofacial bone are in need.

BP particles used in human therapy are mostly obtained from porcine or bovine bones that are subjected to freeze-drying or deproteinization procedures [10]. However, bone particles obtained from non-mammalian vertebrates [13] or from invertebrate species are very rarely evaluated. In this milieu, a promising source of mineralized particles are the echinoderms and, especially, the holothurians. Although holothurians or sea cucumbers are devoid of a real skeleton, the skin of these animals contains a high number of calcified endodermal ossicles that are synthetized by developing cells and remain joined to muscle and connective cells [14]. Although the exact structure and chemical composition of these ossicles is not well known, it has been described that these structures mainly consist of calcium carbonate ($CaCO_3$) crystals enriched in several ions, such as iron and magnesium [15]. Both the shape and size of these ossicles are highly variable among and within species, and both characters can be used to identify the different species of holothurians [16]. In general, the size of these ossicles ranges between 10 and 500 μm, and most specimens contain a combination of perforated rods, plates, disks, towers, and other types of ossicles. The unique shape, size and surface roughness of these particles make them potential biomaterials for use in bone regeneration [16,17].

In the present study, we evaluated the holothurian ossicles (HOLO) as novel biomaterials for bone regeneration using an *ex vivo* and *in vivo* approach combining several histological, histochemical and immunohistochemical methods to determine the potential usefulness of this novel biomaterial for use in tissue engineering. *Ex vivo* analyses allowed us to determine the biocompatibility of HOLO, whereas *in vivo* grafting in Wistar rats was used to assess the biological effects of this biomaterial and its potential regenerative usefulness in a model of mandible bone defect.

Materials and Methods

Cell Cultures

Cell cultures were generated from human oral mucosa biopsies obtained from healthy donors subjected to minor oral treatments, as previously reported [8]. Biopsies were washed in phosphate-buffered saline (PBS) (D8662, Merck, Darmstadt, Germany) and subjected to enzymatic digestion using a 2 mg/mL solution of type I collagenase from *Clostridium histolyticum* (17100017, Gibco, Waltham, MA, USA) for 6 h at 37 °C. Isolated human oral mucosa fibroblasts were obtained by centrifugation and cultured on culture flasks using Dulbecco's Modified Eagle Medium (DMEM) supplemented with 10 % fetal bovine serum and 1 % antibiotics-antimycotics (A5955, Merck). Subconfluent cells were subcultured using a trypsin-ethylenediaminetetraacetic acid (EDTA) solution (T3924, Merck).

Preparation of HOLO Biomaterials

Novel holothurian ossicles (HOLO) particles were obtained by treating the skin of 2 specimens of *Holothuria sp.* acquired at the local fish market using the hypochlorite method, as previously described [16]. In brief, dead animals were rinsed in water, cut into small fragments and submerged in 5 % sodium hypochlorite for 4–6 h to disaggregate the organic tissues and release the inorganic HOLO particles to the solution. This procedure was carried out in a glass decanter to allow the particles to fall to the bottom, where they were harvested, transferred to a clean tube, and washed several times in tap water and, finally, in distilled water to remove all rests of sodium hypochlorite. HOLO particles were washed in 70 % ethanol for sterilization, and dried. Approximately, 0.5–1.0 grams of particles were obtained per specimen, mainly consisting of a mixture of perforated plates and towers, with an average size of 185 $\pm$ 75 μm $\times$ 50 $\pm$ 15 μm (Fig. 1). In order to compare HOLO particles with a filling material commonly used in human clinic when a bone defect must be filled and autografts are not available, we used commercially available SUS-OSS bone mineral particles (BP) generated by decellularizing porcine bone xenografts (InBiomed, Cordoba, Argentina) [18]. Both types of particles were analyzed using light microscopy with non-polarized and polarized light, and scanning electron microscopy (SEM), as described below.

Evaluation of the Ex Vivo Biocompatibility of Novel HOLO Biomaterials

Biocompatibility of the HOLO particles was assessed *ex vivo* by culturing human fibroblasts in the presence of these particles, both in direct and indirect contact, as previ-

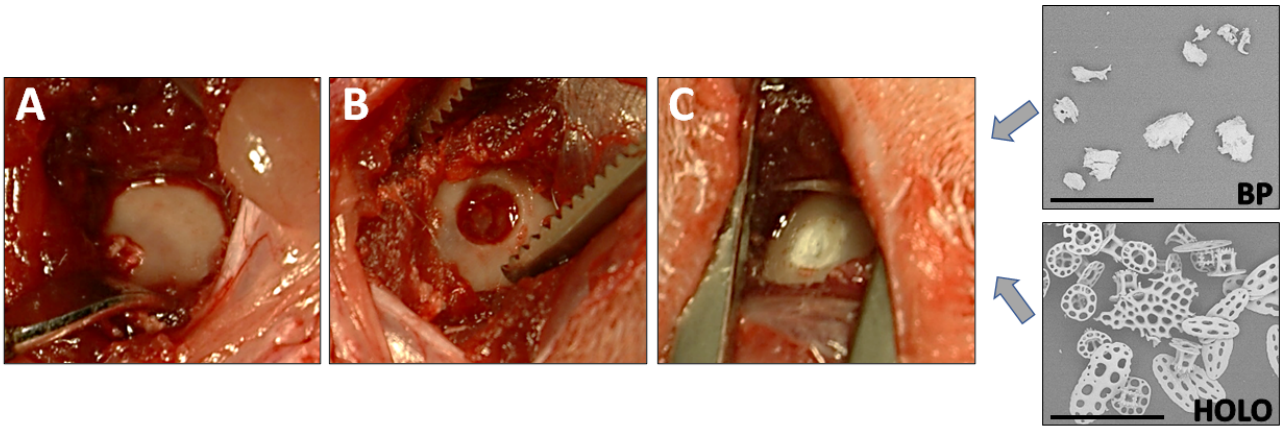

Fig. 1. Surgical procedure carried out on the mandible bone of the laboratory rats included in the present study. (**A**) Surgical exposure of the angle of the mandible at the left side, after separating the muscles originally attached to the bone. (**B**) Generation of a rounded full-size defect in the exposed mandible bone. (**C**) Filling of the bone defect with the HOLO or BP biomaterials analyzed in the present work. At the right side, scanning electron microscopy images of the commercial bone mineral particles (BP) and holothurian ossicles (HOLO) are shown. Scale bars: 200 μm for BP and 100 μm for HOLO.

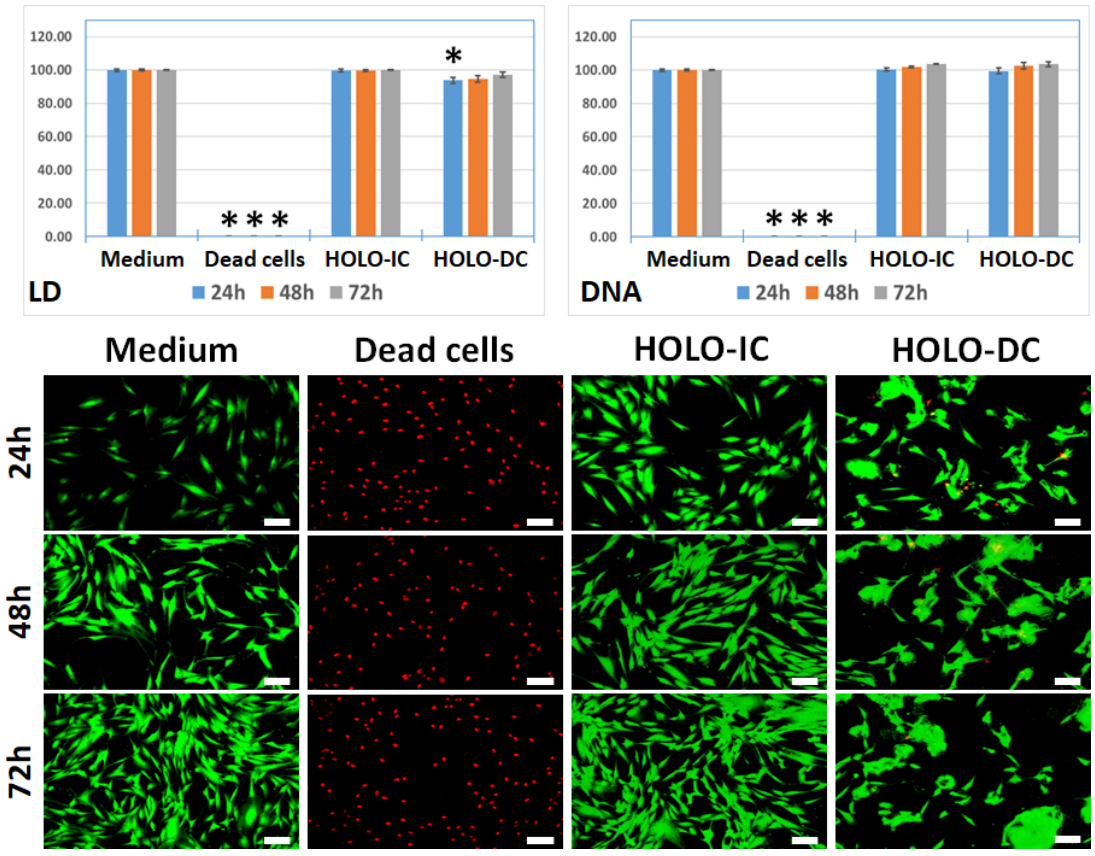

Fig. 2. Analysis of cell viability of human oral mucosa fibroblasts cultured in the presence of holothurian ossicles (HOLO) and control conditions. The top panel shows the histograms corresponding to the quantitative assessment of cell viability using the LIVE/DEAD (LD) technique and free DNA quantification method (DNA) after 24, 48 and 72 h of follow-up. Medium: positive control of cells incubated in culture medium showing 100 % cell viability; Dead cells: negative control of cells treated with triton X-100 showing 0 % cell viability; HOLO-IC: cells cultured in indirect contact with HOLO using porous inserts; HOLO-DC: cells cultured in direct contact with HOLO. Values in the histograms correspond to average cell viability levels normalized to positive and negative controls, and statistically significant differences with the Medium group are highlighted with asterisks (*). The lower panel shows illustrative images of cells analyzed with LIVE/DEAD for each group of study and each incubation time. Live cells are stained in green, whereas dead cells appear in red color. Scale bars: 100 μm.

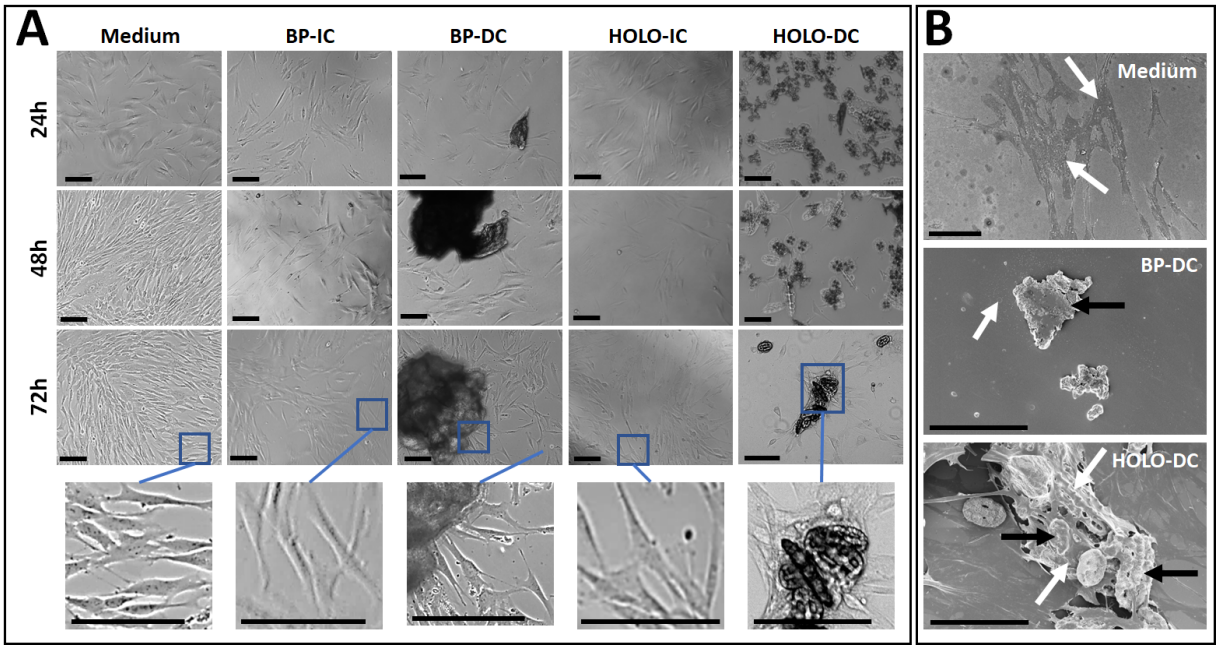

Fig. 3. Illustrative images of human fibroblasts cultured in the presence of holothurian ossicles (HOLO) and controls. (**A**) Phase contrast microscope images. (**B**) Scanning electron microscopy (SEM) images. Medium: control cells incubated in culture medium without particles; BP-IC: cells cultured in indirect contact with the bone mineral particles (BP); BP-DC: cells cultured in direct contact with BP; HOLO-IC: cells cultured in indirect contact with HOLO; HOLO-DC: cells cultured in direct contact with HOLO. High-magnification images in (A) correspond to the inserts in the images at 72 h. In (B), white arrows are used to highlight cultured cells, whereas black arrows show BP or HOLO particles. Scale bars: 100 μm.

ously described [19].

For the indirect contact study of *ex vivo* biocompatibility of HOLO particles [19], cells were cultured on the bottom of 24-well culture plates (50,000 cells per well of 1.9 cm^2 of area surface) and allowed to attach for 24 h in a cell culture incubator. Then, porous culture inserts (140627, Nunc-Thermo Fisher Scientific, Waltham, MA, USA) were placed on each well, and 10 mg of HOLO particles were deposited on the surface of the porous membrane in each insert to allow them to contact the culture medium in which cells were cultured. For the direct contact study, cells were cultured at the same concentration in the same culture plates, but particles were added directly on the culture wells, without using porous culture inserts. The concentration of particles in the direct contact assays was the same that we used for the indirect contact study. In both cases, the effects of the HOLO particles were analyzed after 24, 48 and 72 h of incubation. Two control groups were also established: cells cultured in culture medium (Medium group) without particles were considered as a positive control of cell viability, whereas cells treated with 2 % triton X-100 (9036-19-5, Merck, Darmstadt, Germany) showing 0 % cell viability were considered as negative control of cell viability (Dead cells group). 10 experimental replicates were used per study group (n = 10).

Cell viability of cells incubated with HOLO was first assessed at each incubation time using LIVE/DEAD (LD) cell viability/cytotoxicity kits (L3224, Life Technologies, Carlsbad, CA, USA), following the manufacturer's recommendations [19]. In brief, cells were washed in PBS and cultured for 15 min in a solution containing acetomethoxycalcein and ethidium bromide in PBS. This solution was then removed, and cells were washed in PBS and examined using a ZOE Fluorescent Cell Imager (1450031, Bio-Rad, Hercules, CA, USA). Green viable cells and red dead cells were counted in each experimental condition, and the percentage of viable cells regarding the total number of cells was calculated. Then, cell viability was analyzed by quantifying free DNA released to the culture medium by dead cells, as previously described [19]. In brief, the supernatant culture medium was harvested from each culture well, and the absorbance at 260/280 nm was determined using a NanoDrop 2000 spectrophotometer (ND-2000C, Thermo Fisher Scientific, Waltham, MA, USA) to obtain the final concentration of DNA in each sample. For LD and DNA quantification, results obtained in each study group were normalized against the controls using the results obtained in the Medium group as 100 % cell viability and the results of the Dead cells group as 0 %, as previously reported [20,21].

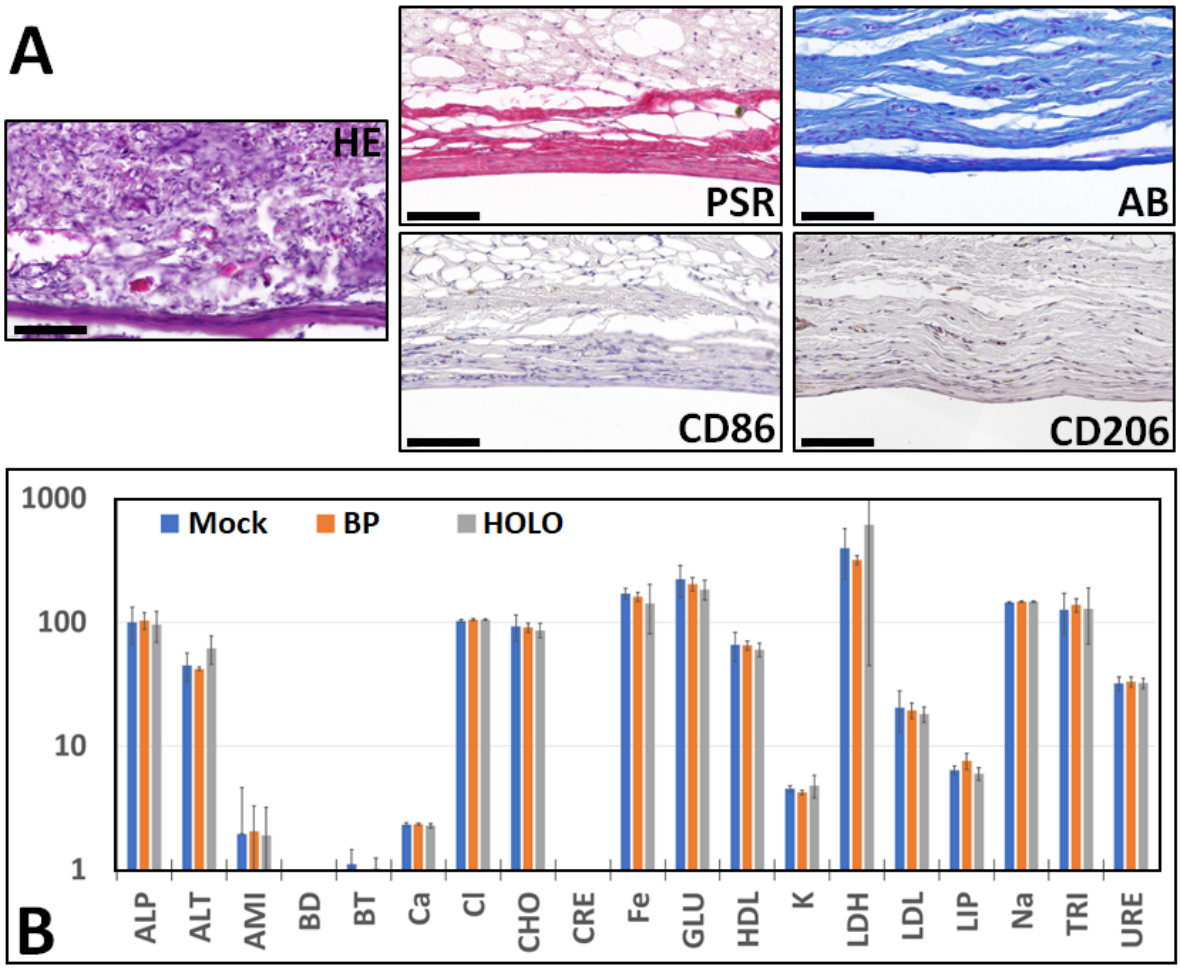

Fig. 4. Evaluation of biocompatibility *in vivo* of the HOLO biomaterial grafted subcutaneously in laboratory rats. (**A**) Histological analysis of the graft site using hematoxylin-eosin (HE) staining, histochemistry for picrosirius red (PSR) and alcian blue (AB) and CD86 and CD206 immunohistochemistry. Scale bars: 100 μm. (**B**) Analysis of biochemical parameters in plasma of animals grafted with HOLO particles. Animals grafted with BP and control animals without any particles (Mock) are also shown. ALP, alkaline phosphatase (in U/L); ALT, alanine transaminase (in U/L); AMI, amylase (in U/L); BD, direct bilirubin (in mg/dL); BT, total bilirubin (umol/L); Ca, calcium (mmol/L); Cl, chlorine (mmol/L); CHO, cholesterol (mg/dL); CRE, creatinine (mg/dL); Fe, iron (ug/dL); GLU, glucose (mg/dL); HDL, high-density lipoprotein (mg/dL); K, potassium (mmol/L); LDH, lactate dehydrogenase (U/L); LDL, low-density lipoprotein (mg/dL); LIP, lipase (U/L); Na, sodium (mmol/L); TRI, triglycerides (mg/dL); URE, urea (mg/dL). Histogram bars represent average values in logarithmic scale, and error bars correspond to standard deviations.

Phenotypic Characterization of Human Cells Cultured with HOLO Biomaterials

In order to evaluate the effects of HOLO on cell morphology, and to assess the interaction between the cultured cells and the biomaterials, cells were directly cultured with HOLO particles. Human fibroblasts were subcultured on 24-well culture plates as described above for the *ex vivo* biocompatibility studies, and HOLO particles were added directly on each culture well (for direct contact studies) or on the surface of porous culture inserts (for the indirect contact studies). As controls, cells cultured in culture medium without particles were used as a positive control of normal cell morphology (Medium group), and cells treated with BP particles in direct or indirect contact were used. The same conditions were used for all study groups. Cells were examined after 24, 48 and 72 h of incubation using an Eclipse Ti-U inverse phase contrast microscope, and microphotographs were obtained from each experimental condition to evaluate cell morphology. After 72 h, cells were fixed *in situ* using 3 % glutaraldehyde, washed three times in cacodylate buffer, dehydrated with increasing concentrations of acetone (30 %, 50 %, 70 %, 95 % and 100 %) and dried using the critical point methods. Samples were then covered with gold using a sputter coater and examined using a FEI scanning electron microscopy (SEM, Quanta 200, FEI, Hillsboro, OR, USA). For both, the phase contrast microscope and SEM images,

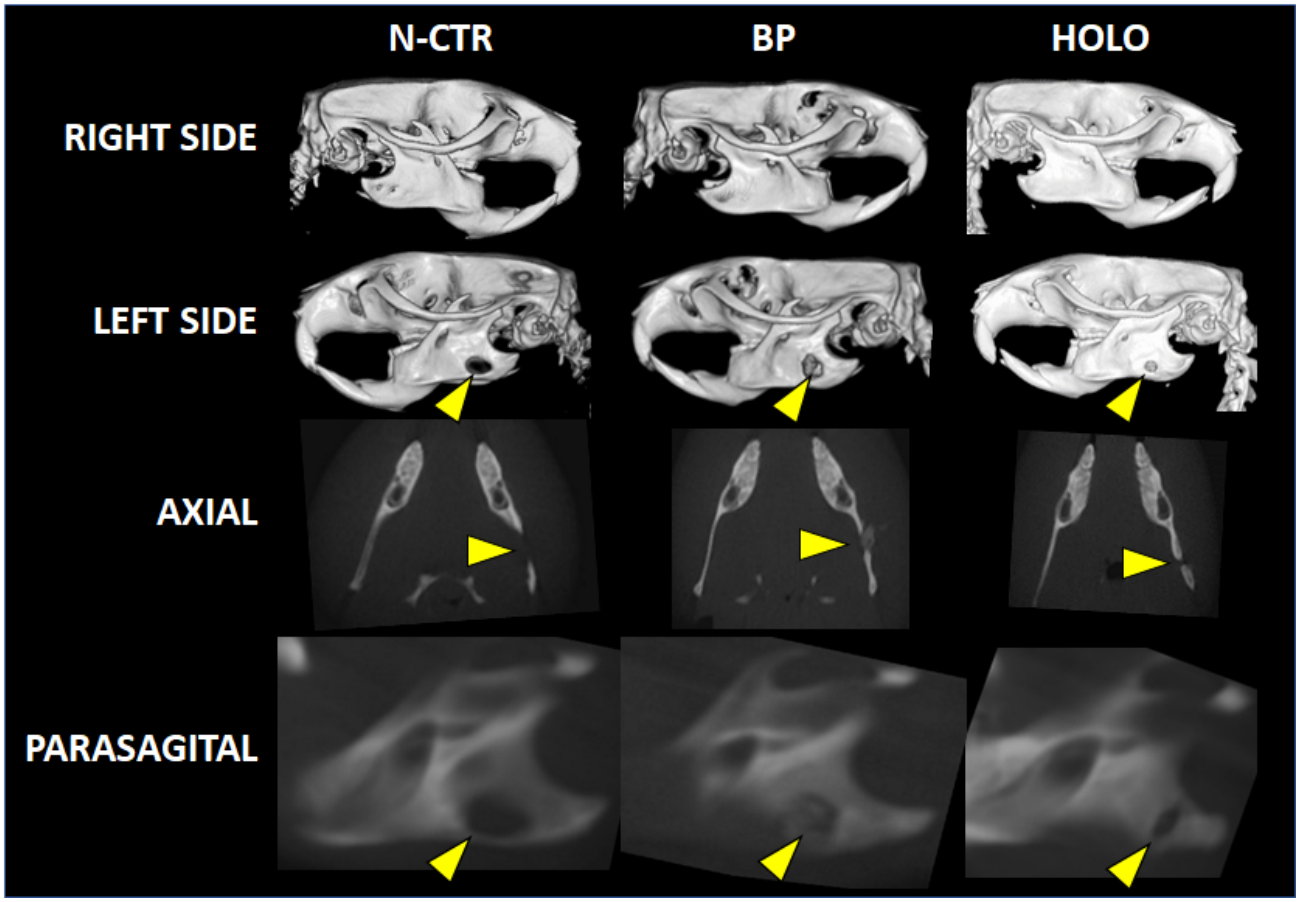

Fig. 5. Cone beam computed tomography (CT) evaluation of animals subjected to mandibular bone defects and treated with holothurian ossicles (HOLO). N-CTR: negative control animals in which the bone defect was not filled by any grafted material; BP: animals in which the bone defect was filled with commercially available bone mineral particles (BP) used clinically; HOLO: animals in which the bone defect was filled with HOLO particles. For each animal, illustrative images corresponding to the three-dimensional (3D) reconstruction of the craniofacial bones and tomographic sections at the grafting site are shown. Right side: 3D reconstruction observed from the non-operated side of the mandible used as normal controls; Left side: 3D reconstruction observed from the operated side of the mandible showing the mandible defect after 2 months of follow-up; Axial: tomographic section in the axial plane showing the defect at the right side of the mandible bone; Parasagital: tomographic section of the operated side of the mandible in the parasagittal plane showing the bone defect. Arrowheads point to the mandible defect in each animal.

the histological appearance of each cell and their relationship with the particles were evaluated.

Evaluation of the In Vivo Biocompatibility of HOLO Biomaterials

In vivo biocompatibility of the different HOLO biomaterials was carried out in adult 12-week-old male Wistar rats weighing approximately 300 g, as suggested for the evaluation of these products [22]. Animals were purchased from Envigo (Indianapolis, IN, USA), and maintained in the animal experimentation unit of Instituto de Investigación Biosanitaria ibs.GRANADA under veterinary supervision, following national guidelines for animal experimentation. Animals were maintained in individual cages in a pathogen-free facility with free access to water and food (commercial irradiated rat chow).

In brief, 5 animals were deeply anesthetized using ketamine and acepromazine, and a subcutaneous pouch was surgically generated at the dorsal area of each animal. Then, 50 mg of HOLO particles were placed on the subcutaneous pouch, using a silicon ring to prevent the particles from moving from the implant site. The skin injury was then sutured using resorbable materials. After 60 days of follow-up, animals were euthanized by injecting a euthanasia solution (Eutanax 200, Fatro Ibérica, Barcelona, Spain) under general anesthesia. The implant site was then carefully dissected and evaluated to detect any sign of rejection, infection, necrosis, or other type of possible side effect of the grafted particles, and these tissues were fixed and processed for histological analysis as described below.

In addition, blood samples were obtained from each animal, and the following biochemical parameters were quantified in plasma using a clinical chemistry analyzer (Cobas c311, Roche, Basel, Switzerland): alkaline phos-

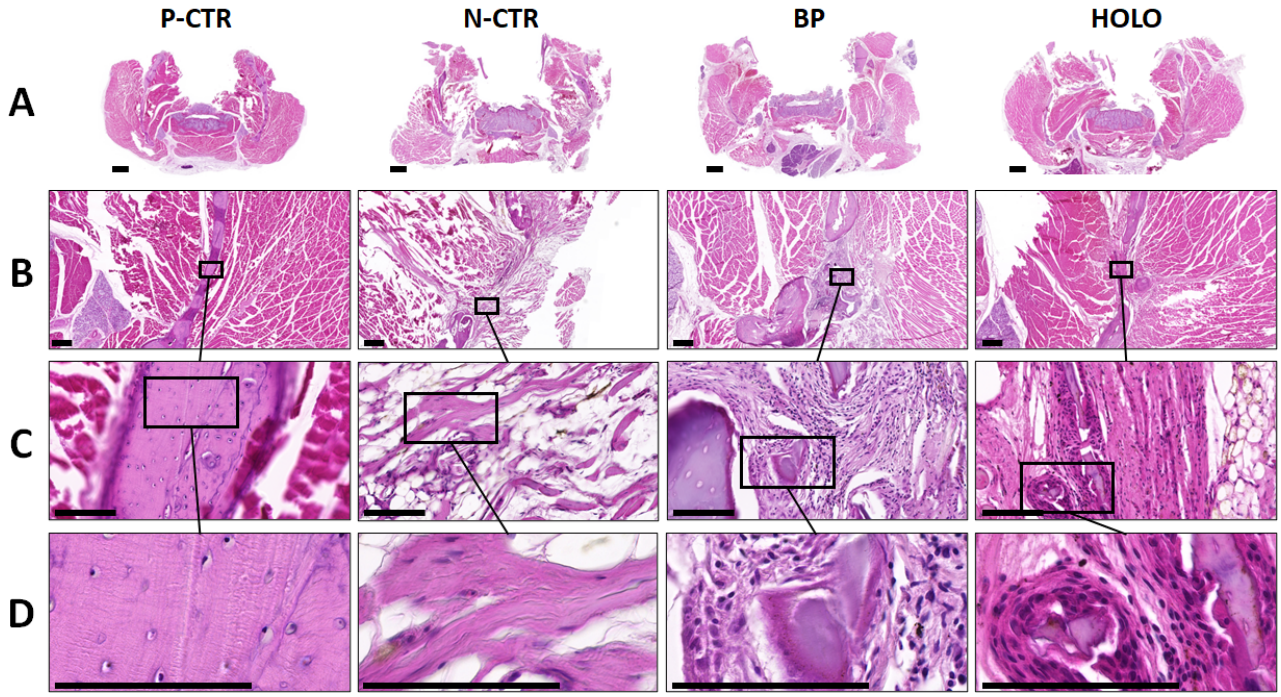

Fig. 6. Histological analysis of the mandible bone of the animals included in the study stained with hematoxylin-eosin (HE). P-CTR: positive control of native, non-operated animals; N-CTR: negative control animals in which the bone defect was not filled by any grafted material; BP: animals in which the bone defect was filled with commercially available bone mineral particles (BP) used clinically; HOLO: animals in which the bone defect was filled with HOLO particles. The top panel (**A**) corresponds to the low-magnification images showing both sides of the mandible. Lower panels (**B–D**) show higher magnification images of the left side of the mandible at different magnifications to show the defect site. Scale bars: 2000 μm in (**A**), 500 μm in (**B**) and 100 μm in (**C,D**) panels.

phatase (in U/L), alanine transaminase (in U/L), amylase (in U/L), direct bilirubin (in mg/dL), total bilirubin (umol/L), calcium (mmol/L), chlorine (mmol/L), cholesterol (mg/dL), creatinine (mg/dL), iron (ug/dL), glucose (mg/dL), high-density lipoprotein (mg/dL), potassium (mmol/L), lactate dehydrogenase (U/L), low-density lipoprotein (mg/dL), lipase (U/L), sodium (mmol/L), triglycerides (mg/dL), and urea (mg/dL). For the biochemical analyses, animals in which BP were grafted using the same procedure, along with control animals (Mock group) in which the surgical procedure was carried out without grafting any particles, were also evaluated (5 animals per group). As this was a preliminary exploratory study, a sample size associated to a specific statistical power could not be calculated.

Evaluation of the In Vivo Functionality of HOLO Biomaterials

In vivo functional analyses of HOLO particles were performed by grafting these particles in an animal model of Wistar laboratory rats in which a critical mandibular bone defect was created, as previously published [23]. Animals were deeply anesthetized by intraperitoneal injection of ketamine and xylazine, and the angle of the left side of the mandible was surgically exposed using blunt dissection to separate the masticatory muscles. A critical-size bone defect of 5 mm of diameter was generated at the mandible angle using a trephine (Fig. 1). The mandibular defect was then filled with HOLO particles (HOLO group), the muscles and soft tissues were repaired, and the skin injury was sutured using resorbable suture material. As controls, the bone defect was filled with BP material (BP group) or was left unfilled in the negative control group (N-CTR group). Native rats not subjected to any surgical procedure were considered as positive controls (P-CTR group). 5 animals randomly selected were included in each group (n = 5).

After 2 months of follow-up, animals were euthanized by intraperitoneal injection of euthanasia solution under general anesthesia, and the oral and maxillofacial skeleton was analyzed by cone beam computed tomography (CT). For this, the head of each animal was scanned with a Dental Imaging System (PointNix Point 3D Combi 500C, Abex Medical System, Shah Alam, Selangor Darul Ehsan, Malaysia) using a high-resolution scanning mode. Then, images were processed to obtain 3D reconstructions of the head and mandible bones, and photographs were taken from the right side (non-operated) and from the left side (operated side) in each group of animals. In addition, axial and parasagittal sections of the mandibular bone were obtained at the site of the defect. These images were used to quantify the size of the bone defect using 3 technical measures from each individual.

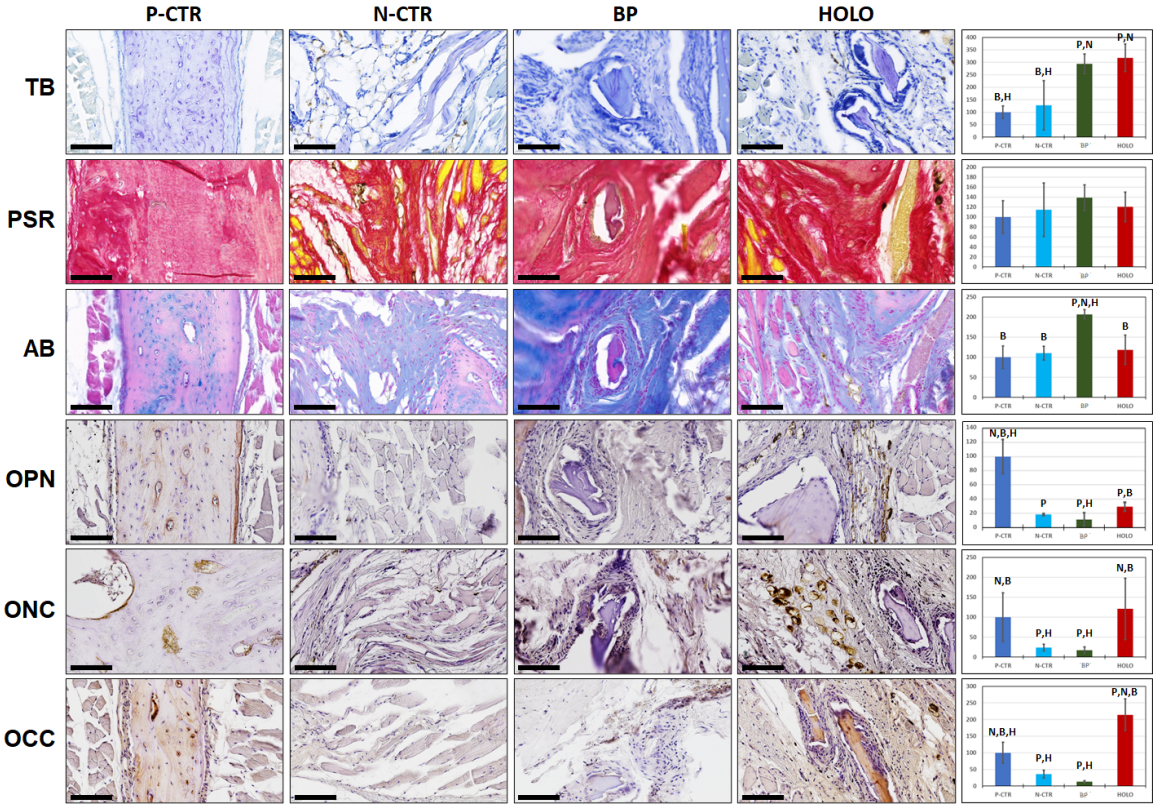

Fig. 7. Histochemical and immunohistochemical evaluation of the mandible bone of the animals included in the study. P-CTR: positive control of native, non-operated animals; N-CTR: negative control animals in which the bone defect was not filled by any grafted material; BP: animals in which the bone defect was filled with commercially available bone mineral particles (BP) used clinically; HOLO: animals in which the bone defect was filled with HOLO particles. TB, toluidine blue; PSR, picrosirius red; AB, alcian blue; OPN, osteopontin; ONC, osteonectin; OCC, osteocalcin. Histograms to the right correspond to the quantitative analysis of each staining method. P: differences with P-CTR are statistically significant, N: differences with N-CTR are statistically significant, B: differences with the BP group are statistically significant, H: differences with the HOLO group are statistically significant. Scale bars: 100 μm.

Histological, Histochemical and Immunohistochemical Analyses

For histological analysis, the implant site of animals used for the *in vivo* biocompatibility studies (subcutaneous tissue) and the *in vivo* functionality (head of the animals) were fixed in 10 % buffered formalin (252931, PanReac Química, Barcelona, Spain) for 24–48 h. In the case of the animal heads, decalcification was carried out using Anna Morse (50 % formic acid and 20 % sodium citrate in water) (PanReac Química, Barcelona, Spain) for 6–7 days or until the hard tissues became soft [24]. The mandible bone and the soft tissues attached to the mandible were carefully dissected and separated from the rest of the cranial structures, and serial gross sections with an approximate thickness of 5 mm were obtained in the coronal plane with a surgical blade, from the most frontal to the most dorsal part of the mandible, including both mandibular rami (control right side and operated left side) in each section. Gross sections were then washed, dehydrated in ethanol series, cleared in xylene, and embedded in paraffin. Thin tissue sections with a thickness of 4 μm were obtained with a microtome, dewaxed in xylene and rehydrated for histological evaluation. To evaluate the global histological structure and host response to grafted materials, slides were stained with hematoxylin-eosin (HE) using routine methods. After examining each slide, the tissue blocks corresponding to the area of the surgical intervention at the mandibular region were selected for further analysis. Control and study animals were subjected to the same procedure.

In the blocks corresponding to the area of the surgical intervention, relevant extracellular matrix (ECM) components were analyzed histochemically [25,26]. For collagen fibers, picrosirius red (PSR) was used by incubating the slides in a Sirius Red F3B solution for 30 min, washing in water and counterstaining in Harris Hematoxylin (72711, Thermo Fisher Scientific, Waltham, MA, USA) for 15 s. For proteoglycans, alcian blue (AB) histochemical methods were used by treating the slides in alcian blue working solution at pH 2.5 for 30 min, followed by washing in water and counterstaining with nuclear fast red for 1 min. For the identification of osteoid tissue, corresponding to immature bone mainly consisting of poorly-mineralized organic ma-

terial, toluidine blue (TB) was used. In brief, samples were treated with toluidine blue solution for 2–5 min, washed in acetate-acetic buffer at pH 4.2, treated with molybdate for 5–10 min and washed in tap water. All these reagents were purchased from PanReac Química (254584 for AB, A8020.0005 for nuclear fast red, 251176 for TB, 131632 for acetate-acetic, and 131134 for molybdate; Barcelona, Spain).

Specific markers of bone differentiation, including osteopontin (OPN), osteonectin (ONC) and osteocalcin (OCC), and proteins of M1 and M2 macrophage phenotypes (CD86 and CD206, respectively) were identified by indirect immunohistochemistry. Briefly, tissue sections were subjected to antigen retrieval, and endogenous peroxidases were quenched with H_2O_2 (131077.1211, PanReac Química, Barcelona, Spain). Prehybridization was then performed with casein and normal horse serum (S-2012-50, Vector laboratories, Burlingame, CA, USA), and samples were incubated overnight at 4 °C with the primary antibodies at the following dilutions: 1:500 for OPN, 1:250 for ONC, 1:50 OCC, 1:200 for CD86 and 1:800 for CD206. A prediluted solution containing the secondary antibodies labeled with peroxidase was then applied, followed by a diaminobenzidine (DAB) substrate kit (SK-4100, Vector Laboratories) to reveal the staining reaction. Samples were finally counterstained with Harris Hematoxylin (Thermo Fisher Scientific, Waltham, MA, USA) for 15 s, and coverslipped.

Histological images were obtained from each slide using a histological scanner (Pannoramic Desk DW II, 3DHISTECH, Budapest, Hungary).

Staining Signal Quantification and Statistical Analyses

Images corresponding to the histochemical and immunohistochemical staining methods were analyzed to quantify the staining signal using the ImageJ software (version 1.54g, National Institute of Health, Bethesda, MD, USA), as previously reported [27,28]. For the histochemical analyses (PSR, AB and TB) and for the immunohistochemical analysis of bone differentiation markers (OPN, ONC and OCC), 10 dots were randomly assigned to each histological image using the multi-point tool of the program, and the signal intensity was automatically calculated for each dot and expressed in color intensity units (I.U.). For the immunohistochemical evaluation of CD86 and CD206 markers, the number of stromal cells showing positive signal for each of these markers was determined in each sample. Quantification was carried out in a blinded manner, so that researchers did not know the specific type of sample that was quantified for each method.

For statistical analysis, we first evaluated if each variable fits a normal distribution using the Shapiro-Wilk test. As variables could be considered as normal, parametric statistics was applied. Statistical comparison of the size of the bone defect in the different study groups of the *in vivo* functionality study was performed using analysis of variance (ANOVA) for global comparison of multiple groups with a post-hoc pairwise comparison between two specific groups using the honestly-significant-difference (HSD) test of Tukey. The same statistical tests were used to compare the quantitative results of the histochemical and immunohistochemical analyses. In the case of the LD and DNA release results, comparisons between two groups were carried out using the exact test of Fisher, as results were expressed as percentages. All comparisons were carried out double-tailed, and a statistical p value below 0.05 was considered as statistically significant. Statistical tests were performed using the Real Statistics Resource Pack software (Release 7.2) (Dr. Charles Zaiontz, Purdue University, West Lafayette, IN, USA), available at https://real-statistics.com.

Results

Ex Vivo Biocompatibility of HOLO Biomaterials

In the first place, we analyzed the *ex vivo* biocompatibility of the HOLO biomaterial using LIVE/DEAD assays. As shown in Fig. 2 and **Supplementary Table 1**, cells cultured in indirect contact with HOLO were highly viable, with no differences with control viable cells (Medium group), and with significant differences with the Dead cells group. When the human cells were cultured in direct contact with HOLO, we found that cell viability was above 93% at all study times, although differences were significant at 24 h, and viability tended to increase with the follow-up time. Then, we assessed cell viability by free DNA quantification. Results found that cells were highly viable after 24, 48 and 72 h, and differences with the Medium group of viable cells were not statistically significant.

Phenotypic Characterization of Human Cells Cultured with HOLO Biomaterials

As shown in Fig. 3, we found that control human cells cultured without particles (Medium group) showed the typical spindle-shape, elongated morphology of normal stromal cells both in phase contrast microscope and SEM. In addition, our morphological analysis of cells cultured in indirect contact with HOLO and with BP biomaterials revealed no morphological differences with P-CTR, with cells displaying a normal morphology in all cases. Interestingly, when cells were cultured in direct contact with BP, we found that most cells showed the typical morphology of this type of cells, but fibroblasts tended to adhere to the culture flask surface rather than to the particles of the biomaterial. However, cells cultured in direct contact with HOLO tended to adhere to the biomaterial and formed clusters containing cells and HOLO particles attached together, whereas the culture surface devoid of HOLO particles tended to show lower cell concentrations.

In Vivo Biocompatibility of HOLO Particles

Histological evaluation of HOLO biomaterials grafted subcutaneously in laboratory animals using HE (Fig. 4**A**) showed that HOLO particles tended to remain at the implant site, without any detectable sign of necrosis, host rejection, inflammation, or tumorigenesis in any of the animals. No adverse effects were found. When the grafting site was analyzed using PSR histochemistry, we found a thin PSR-positive collagen-rich pseudocapsule surrounding the connective tissue in which HOLO were implanted, but no signs of fibrosis or adhesions were detected. Analysis of the grafting site using AB histochemistry revealed a highly positive staining signal for this histochemical method, suggesting the presence of abundant proteoglycans both in the pseudocapsule and in the inner tissue. When the macrophage population was analyzed at the implant site, we found very few cells showing CD86 positive expression corresponding to pro-inflammatory M1-type macrophages, and abundant pro-regenerative M2-type macrophages showing positive expression of CD206.

In addition, the analysis of relevant biochemical parameters in blood of the animals grafted with HOLO materials showed no differences with the Mock group of control rats ($p > 0.05$ for all parameters). Similarly, the biochemical results found in animals grafted subcutaneously with BP were statistically comparable to the Mock group and to the HOLO group for all the analyzed parameters, with differences being statistically non-significant (Fig. 4**B**).

In Vivo Functionality of HOLO Particles

To evaluate the potential usefulness of HOLO materials in mandible bone regeneration, we carried out *in vivo* experiments on laboratory animals in which a critical mandibular bone defect had been generated (Fig. 5). In the first place, our results revealed that N-CTR animals in which the mandible defect was not filled by any biomaterial showed large defects at the end of the follow-up time, with an average size of 9.16 ± 4.18 mm. This defect was evident in the 3D reconstructions of the craniofacial bones of the animals and in the axial and parasagittal tomographic sections displayed in Fig. 5. In the second place, we found that BP animals in which the bone defect was filled with bone mineral particles used clinically showed positive results as compared to N-CTR, and the average size of the bone defect was 6.31 ± 2.93 mm, corresponding to 68.95 ± 32.05 % of the average size of the defect found in N-CTR. Although differences between BP and N-CTR did not reach statistical significance ($p = 0.2911$), the morphological analyses carried out using 3D reconstructions and sections of the mandible bone revealed an improvement as compared to N-CTR. Finally, evaluation of animals in which the bone defect was filled with holothurian particles (HOLO group) showed a significant reduction in the size of the bone defect (average 3.36 ± 0.84 mm, corresponding to 36.67 ± 9.14 % of N-CTR), with statistically significant differences with N-CTR ($p = 0.0122$). As revealed by the CT analysis, the bone defect found in the HOLO group was smaller than that found in N-CTR and BP, although differences with the BP group were not statistically significant ($p = 0.2659$).

In Vivo Histological Analysis

Histological analysis of the mandible bone of animals included in the study revealed several differences among groups. As shown in Fig. 6, the structure of the mandible bone corresponding to the P-CTR group of native animals was compatible with a normal compact bone containing abundant osteocytes surrounded by a dense mineralized extracellular matrix. Then, the N-CTR group showed an important defect at the left side of the mandible, and this defect contained abundant connective tissue consisting of numerous fibroblasts and a dense extracellular matrix with thick, mature collagen fibers. No signs of ossification were found in this connective tissue. When the BP group was analyzed, we found that the induced defect was detectable at the left side of the mandible. This defect was filled with a very dense, collagen-rich connective tissue with abundant cells, and several areas of calcification partially resembling the histological structure of the compact bone were found at this level, although these particles were mostly surrounded by the connective tissue. Some of the grafted particles showing empty osteocyte lacunae were visible. Finally, the histological analysis of the HOLO group of animals also revealed the presence of the induced bone defect at the left side of the mandible containing a very dense connective tissue with abundant cells and collagen fibers. Several spots of calcification compatible with mineralized tissue were found within and partially surrounded by this connective tissue.

Then, we analyzed the composition of the tissue found at the mandible defect of each study group using histochemistry and immunohistochemistry (Fig. 7 and **Supplementary Table 2**). First, the assessment of osteoid tissue formation using toluidine blue (TB) histochemistry showed very low staining signal in P-CTR and N-CTR. However, we found that the mineralized spots found in the BP and the HOLO groups were TB-positive, with significantly higher staining intensity than P-CTR and N-CTR ($p < 0.0001$ for both groups), whereas BP and HOLO were statistically similar to each other ($p > 0.05$). When the ECM was analyzed in each study group, we found that all groups contained abundant amounts of collagen fibers identified by PSR staining, with non-significant differences among groups ($p > 0.05$), whereas proteoglycans detected by AB were significantly more abundant in the BP group ($p < 0.0001$), whilst the P-CTR, N-CTR and HOLO groups were statistically similar ($p > 0.05$).

In addition, our immunohistochemical analysis of three specific bone proteins (Fig. 7) revealed several differences among the four study groups compared in the present study. For osteopontin (OPN), our results showed that P-CTR had significantly higher levels of this protein than the

N-CTR, BP and HOLO groups ($p < 0.0001$), and the regeneration tissue found in the HOLO group showed higher contents of OPN than the BP group ($p = 0.0232$). Evaluation of osteonectin (ONC) showed that the HOLO group expressed similar levels of this protein than the P-CTR, with P-CTR and HOLO showing significantly higher contents than N-CTR ($p = 0.0078$ and $p = 0.0006$, respectively) and BP ($p = 0.0035$ and $p = 0.0002$, respectively). In turn, the osteocalcin (OCC) staining signal found in the HOLO group was significantly more intense than all the other study groups ($p < 0.0001$), and N-CTR and BP were significantly lower than P-CTR ($p < 0.0001$).

Discussion

The recent development of bone tissue engineering protocols may provide regenerative approaches to the treatment of severe defects of the human mandibular bone [29], and several biomaterials were previously tested with variable results [7,8,30]. In general, the use of BP in bone augmentation and bone repair became increasingly popular, due to the promising results obtained with these biomaterials [10,11,31]. However, novel biomaterials able to improve the clinical results of BP should be developed.

In the present work, we evaluated the biological effects of a novel natural biomaterial applied to the regeneration of critical-size mandibular bone defects. This biomaterial can be obtained from an abundant source of marine animals that has been commercially exploited for years for diverse applications, including seafood and pharmaceutical uses [32]. In fact, holothurians are commonly used commercially in several countries, especially in Asia, and efforts are currently made to produce these animals at large scale in aquaculture industries [33].

For clinical translation, novel biomaterials used in regenerative medicine must be characterized at different levels to ensure biosafety and efficiency of these products [34–36]. As recommended for other biomaterials and tissue engineering products, we first evaluated the *ex vivo* effects of HOLO on cell viability. Demonstrating that novel biomaterials are not cytotoxic and do not alter cell viability is a very important prerequisite of products developed for tissue engineering protocols [36,37]. In this regard, we used two different analysis methods to evaluate cell viability, including a functional metabolic assay (LD) and a structural method analyzing cell membrane integrity. Results of the indirect contact analyses confirmed that HOLO particles are safe for the human cells and suggest that these particles do not release any toxic molecules able to impair cell viability. Similar results were found when cells were cultured in direct contact with HOLO, although an initial viability decrease was detected with LD. This temporal and self-limited decrease has been previously described for primary cultures, and could be related to the initial adaptation phase of cultured cells [38]. In agreement with the *ex vivo* biocompatibility results, evaluation of cell phenotype revealed that HOLO were not associated to a morphological change of the cultured cells, suggesting that cell viability was not compromised [39]. Although not human, the fact that HOLO particles were extracted from a natural source, and their composition is a mixture of several types of low-solubility calcium carbonate minerals [40] could explain their biocompatibility when cultured with human cells.

An interesting finding was the different behavior found in cells cultured in direct contact with HOLO as compared to BP. Despite BP are commonly used in clinics, our results showed that the attachment level of human cells to these particles was limited, whereas cell confluence was significantly higher around HOLO particles. Although upcoming studies should characterize the exact surface structure of each type of particle, we may theorize that this differential behavior of cultured cells could be related to the porosity and surface morphology of each type of particles. Whilst BP particles are normally manufactured by fracturing large pieces of bone, and the process could alter the original structure of these materials, HOLO particles were isolated without fragmentation. In this regard, it is important to note that HOLO were obtained using a very simple method that does not alter the native structure of these particles in the animal tissue, where cells are continuously interacting with the particle surface. Again, the natural nature of HOLO ossicles and their native structure could be related to the adequate interaction and attachment of cells cultured in direct contact with HOLO particles. In fact, it has been previously suggested that natural biomaterials obtained from renewable sources have unique biological properties derived from their structure and composition, which may offer excellent biological support for cell attachment and proliferation [41].

Along with cell viability, the analysis of biocompatibility *in vivo* is a crucial translational requirement of medicines agencies for this type of biomedical products [34,36]. In line with the *ex vivo* analyses, we found that HOLO particles were highly biocompatible when grafted on laboratory animals, and no local or systemic side effects were detected in any of the animals, both at the histological and the biochemical level, suggesting that these particles fulfilled the biosafety requirements for clinical use [36].

Once we demonstrated that HOLO particles were safe for *in vivo* use, we analyzed the functional effects of this novel biomaterial on mandible bone regeneration. Results showed that the use of HOLO was associated to a significant improvement of bone regeneration in a model of critical mandible defect. Although the defect was still identifiable at the end of the follow-up time, we found that the bone defect found in the HOLO group corresponded to roughly one-third of the diameter of the control group, with significant differences between both groups of animals, with an evident radiological improvement in HOLO. Interestingly, the diameter of the defect was approximately two-thirds of the control group when commercial BP were used, which

was not significantly different to the control group. These results support the idea that HOLO biomaterials could exert a positive effect on mandible bone regeneration. The fact that regeneration was only partial in all groups of animals could be related to the follow-up time used in the present study. Hence, some previous studies demonstrated that bone mandible defects require long periods of time to regenerate, and critical lesions contain connective tissue after 4 weeks of follow-up [23], although the bone healing process predominantly takes place in the first two weeks after the generation of the defect. In addition, it is important to note that the animal model used in the present study has several limitations related to the different physiology of the rat and human bone tissue, and that the sample size was very low, what typically affects statistical significance. Furthermore, bone regeneration was assessed using CBCT, which is commonly used to evaluate dental and maxillofacial bone regeneration, but its resolution is limited. Future studies should use micro-CT and other high-resolution analysis methods to confirm the results obtained in the present work. An unanswered question is the fact that, for some animals, the diameter of the defect was higher than that of the trephine instrument used to generate the defect in the first place. Most likely, this could be explained by the fact that trephines may typically generate bone defects with slightly higher diameters, due to friction during the procedure, and, especially, by an associated process of bone resorption at the edges of the defect, as previously reported [42]. Although this animal model was previously described for the experimental evaluation of different biomaterials in mandibular regeneration [23], novel *in vivo* models able to more biomimetically reproduce the human scenario should be described.

At the histological level, our results showed that the mandibular defect of negative control animals was filled with a dense connective tissue, compatible with a failure of the mandibular bone to regenerate. In contrast, the BP and HOLO groups showed several calcification spots at the bone defect. In general, we were not able to identify the grafted material (especially, in the case of HOLO) embedded in the newly formed regenerative bone at the edges of the defect, probably due to demineralization, and most of these mineralized areas were surrounded by connective tissue. Although we may hypothesize that these areas could correspond to a bone regeneration process, future studies should be carried out using non-demineralized tissues to determine the osteointegration process of the grafted materials. These results were in agreement with the analysis of ECM composition showing a positive TB signal at the regeneration area of BP and HOLO. Previous researchers demonstrated that newly formed bone spots stain intensely with toluidine blue, whereas native mother bone typically stains in light blue [43]. To determine the quality of the bone tissue formed at the regeneration area, we quantified the presence of relevant ECM components using histochemical and immunohistochemical methods. Results showed that the regenerated bone contained normal amounts of collagen fibers as compared to native bone control tissue. However, differences were found for the amount of proteoglycans, which were comparable to native bone in the HOLO group and significantly higher in the BP group. The role of these ECM components was demonstrated to be crucial in bone regeneration and ECM remodeling, although their exact regulation and modulation is strictly related to their biological functions, such as the organization of a three-dimensional collagen network [44].

In addition, we evaluated the expression of three bone proteins typically associated to bone physiology and homeostasis that play an important role in bone formation, especially at short terms after the generation of a bone defect [45]. Strikingly, our quantification analysis of OCC, OPN and ONC demonstrated that these three proteins were significantly more abundant in the regenerated bone of the HOLO group than in the BP group, and the levels found in HOLO were similar to native bone for ONC. ONC is a glycoprotein involved in tissue remodeling, whose role is fundamental for a proper bone physiology, as this molecule is able to attract and bind calcium ions, along with collagens types I, II, IV and V [46]. The presence of normal amounts of ONC in the regenerative bone formed in the HOLO group suggests that this tissue could be functional, and shares more similarities with native bone than the bone induced by other biomaterials such as BP. Expression of ONC has been observed in newly mineralized bone and its role in bone mineralization has been previously demonstrated [47]. However, its expression is not highly specific of the bone ECM, and this marker has been found expressed by the ECM and cell nuclei of human bone and by different types of cancer [48]. On the other hand, OCC is considered as the most abundant non-collagenous protein of the bone ECM and a good indicator of new bone formation [49], and its presence has been identified during the transition of immature, poorly-mineralized osteoid tissue to mature calcified bone tissue [47]. The increased expression of this component in the HOLO group is in line with the idea that these biomaterials were able to induce mandibular bone regeneration and contributed to improving currently used regenerative therapies. However, the bone newly formed in HOLO contained significantly lower amounts of OPN than control native bone. OPN is a small integrin-binding ligand glycoprotein that is synthesized and secreted by functional osteoblasts and plays a role in cell adhesion and bone ECM mineralization [50]. In addition, OPN is associated to mature bone remodeling and is also expressed by osteoclasts, where it is thought to participate in bone degradation in resorption lacunae [51]. The fact that OPN has been mainly described in highly-mineralized bone, and is mostly absent in osteoid tissue [47,52] could explain the low levels of this protein in regenerating bone corresponding to the HOLO group. These results should be analyzed with care, since it

is well known that ONC, OCC and OPN are crucial markers of early bone formation, and these analyses were carried out after 2 months of follow-up, when the regeneration process is normally reduced. Future studies should be carried out to analyze these markers at shorter follow-up periods.

The above-mentioned histological, histochemical and immunohistochemical analyses were carried out using demineralized tissues, as previously published [8,53]. However, acid decalcification may affect the morphology and composition of biological tissues, and further studies should be performed using non-demineralized samples. These studies should include a thorough characterization of the chemical composition of the mineralized tissue formed at the defect area, in order to determine if this tissue is able to reproduce the definite structure of the native bone.

The mechanisms associated to the positive effects of HOLO both on human cells and laboratory animals should still be identified. However, it is likely that both the surface structure of each type of particle, their chemical composition and particle size may play a relevant role.

Conclusions

In general, the positive results obtained in the present study confirm the biosafety and potential usefulness of the novel HOLO biomaterials and support the development of clinical trials in humans following the requirements of the European Medicines Agency, although further preclinical analyses are in need to confirm these results. As compared to BP particles currently used therapeutically, HOLO may have increased regeneration potential of the mandible bone. Future long-term and time-course studies are still needed to determine the regenerative potential of these biomaterials in human bone regeneration, and to reveal if the bone ossification process can be completed after longer periods of time. In addition, clinical trials should determine the therapeutic usefulness of these novel biomaterials in human patients.

List of Abbreviations

HOLO, holothurian ossicles; BP, bone mineral particles; $CaCO_3$, calcium carbonate; PBS, phosphate-buffered saline; DMEM, Dulbecco's Modified Eagle Medium; SEM, scanning electron microscopy; LD, LIVE/DEAD; CT, computed tomography; HE, hematoxylin-eosin; ECM, extracellular matrix; PSR, picrosirius red; AB, alcian blue; TB, toluidine blue; OPN, osteopontin; ONC, osteonectin; OCC, osteocalcin; DAB, diaminobenzidine; I.U., intensity units; HSD, honestly-significant-difference; ALP, alkaline phosphatase; ALT, alanine transaminase; AMI, amylase; BD, direct bilirubin; BT, total bilirubin; Ca, calcium; Cl, chlorine; CHO, cholesterol; CRE, creatinine; Fe, iron; GLU, glucose; HDL, high-density lipoprotein; K, potassium; LDH, lactate dehydrogenase; LDL, low-density lipoprotein; LIP, lipase; Na, sodium; TRI, triglycerides; URE, urea; 3D, three-dimensional.

Availability of Data and Materials

The data supporting the findings of this study are openly available in the public repository Zenodo at https://zenodo.org/records/10817020, with the DOI number 10.5281/zenodo.10817020 with the license Creative Commons Attribution 4.0 International.

Author Contributions

OOA, EBM, RFV, AEL and MA designed the research study. OOA, EBM, JCA, VC, AMP, MAMP, IG, RFV, AEL, IÁR and MA performed the research. VC, AMP, MAMP, IG, RFV and IÁR contributed to the analysis of the data. All authors contributed to editorial changes in the manuscript. All authors read and approved the final manuscript. All authors have participated sufficiently in the work and agreed to be accountable for all aspects of the work.

Ethics Approval and Consent to Participate

This study was approved by the regional ethics committee CCEIBA (Comité Coordinador de Ética de la Investigación Biomédica de Andalucía), ref. 2044-N-22 (date of approval 13th, February, 2023) and ref. 1961-N-19 (date of approval 28th, November, 2019). All tissue donors provided written informed consent to participate in the study. Animal experimentation was approved by the Ethics Committee for Animal Experimentation in Andalusia (CEEA), protocol code 08/07/2019/123 (date of approval 10th, September, 2019) and 08/07/2019/122 (date of approval 26th, July, 2019).

Acknowledgments

This study is part of the Doctoral Thesis of Elena Bullejos-Martínez. Authors thank Fabiola Bermejo-Casares for her support with the histological, histochemical and immunohistochemical analyses.

Funding

This work was supported by the Spanish "Plan Estatal de Investigación Científica, Desarrollo e Innovación Tecnológica" (I+D+i) of the Spanish Ministry of Science and Innovation (Instituto de Salud Carlos III), Grants FIS PI24/00006, PI21/00980, FIS PI18/00331, FIS PI18/00332 and ICI19/00024 (BIOCLEFT), supported by grant CSyF PI-0442-2019 from Consejería de Salud y Consumo, Junta de Andalucía, Spain, and cofinanced by the European Regional Development Fund (FEDER/ERDF) through the "Una manera de hacer Europa" program, European Union.

Conflict of Interest

The authors declare that the research was conducted in the absence of any commercial or financial relationships that could be construed as a potential conflict of interest. Dr. Chato-Astrain, Dr. Garzón, Dr. Fernandez-Valades and

Dr. Alaminos, are inventors of patent P202031250, broadly relevant to the work.

Supplementary Material

Supplementary material associated with this article can be found, in the online version, at https://doi.org/10.22203/eCM.v049a01.

References

[1] Sroussi HY, Epstein JB, Bensadoun RJ, Saunders DP, Lalla RV, Migliorati CA, *et al*. Common oral complications of head and neck cancer radiation therapy: mucositis, infections, saliva change, fibrosis, sensory dysfunctions, dental caries, periodontal disease, and osteoradionecrosis. Cancer Medicine. 2017; 6: 2918–2931. https://doi.org/10.1002/cam4.1221.

[2] Deng J, Golub LM, Lee HM, Raja V, Johnson F, Kucine A, *et al*. A Novel Modified-Curcumin Promotes Resolvin-Like Activity and Reduces Bone Loss in Diabetes-Induced Experimental Periodontitis. Journal of Inflammation Research. 2021; 14: 5337–5347. https://doi.org/10.2147/JIR.S330157.

[3] Kawahara M, Kuroshima S, Sawase T. Clinical considerations for medication-related osteonecrosis of the jaw: a comprehensive literature review. International Journal of Implant Dentistry. 2021; 7: 47. https://doi.org/10.1186/s40729-021-00323-0.

[4] Tolstunov L, Hamrick JFE, Broumand V, Shilo D, Rachmiel A. Bone Augmentation Techniques for Horizontal and Vertical Alveolar Ridge Deficiency in Oral Implantology. Oral and Maxillofacial Surgery Clinics of North America. 2019; 31: 163–191. https://doi.org/10.1016/j.coms.2019.01.005.

[5] Tzur E, Ben-David D, Gur Barzilai M, Rozen N, Meretzki S. Safety and Efficacy Results of BonoFill first-in-Human, Phase i/IIa Clinical Trial for the Maxillofacial Indication of Sinus Augmentation and Mandibular Bone Void Filling. Journal of Oral and Maxillofacial Surgery: Official Journal of the American Association of Oral and Maxillofacial Surgeons. 2021; 79: 787–798.e2. https://doi.org/10.1016/j.joms.2020.12.010.

[6] Tomas M, Čandrlić M, Juzbašić M, Ivanišević Z, Matijević N, Včev A, *et al*. Synthetic Injectable Biomaterials for Alveolar Bone Regeneration in Animal and Human Studies. Materials. 2021; 14: 2858. https://doi.org/10.3390/ma14112858.

[7] Guo J, Yao H, Li X, Chang L, Wang Z, Zhu W, *et al*. Advanced Hydrogel systems for mandibular reconstruction. Bioactive Materials. 2023; 21: 175–193. https://doi.org/10.1016/j.bioactmat.2022.08.001.

[8] Martin-Piedra MA, Gironés-Camarasa B, España-López A, Fernández-Valadés Gámez R, Blanco-Elices C, Garzón I, *et al*. Usefulness of a Nanostructured Fibrin-Agarose Bone Substitute in a Model of Severely Critical Mandible Bone Defect. Polymers. 2021; 13: 3939. https://doi.org/10.3390/polym13223939.

[9] Hatt LP, Thompson K, Helms JA, Stoddart MJ, Armiento AR. Clinically relevant preclinical animal models for testing novel cranio-maxillofacial bone 3D-printed biomaterials. Clinical and Translational Medicine. 2022; 12: e690. https://doi.org/10.1002/ctm2.690.

[10] Kamadjaja DB, Abidin ZZ, Diana R, Kharis I, Mira Sumarta NP, Amir MS, *et al*. *In Vivo* Analyses of Osteogenic Activity and Bone Regeneration Capacity of Demineralized Freeze-Dried Bovine Bone Xenograft: a Potential Candidate for Alveolar Bone Fillers. International Journal of Dentistry. 2021; 2021: 1724374. https://doi.org/10.1155/2021/1724374.

[11] Starch-Jensen T, Schou S, Terheyden H, Bruun NH, Aludden H. Bone regeneration after maxillary sinus floor augmentation with different ratios of autogenous bone and deproteinized bovine bone mineral an *in vivo* experimental study. Clinical Oral Implants Research. 2023; 34: 1406–1416. https://doi.org/10.1111/clr.14186.

[12] Basyuni S, Ferro A, Santhanam V, Birch M, McCaskie A. Systematic scoping review of mandibular bone tissue engineering. British Journal of Oral & Maxillofacial Surgery. 2020; 58: 632–642. https://doi.org/10.1016/j.bjoms.2020.03.016.

[13] Terzioğlu P, Öğüt H, Kalemtaş A. Natural calcium phosphates from fish bones and their potential biomedical applications. Materials Science & Engineering. C, Materials for Biological Applications. 2018; 91: 899–911. https://doi.org/10.1016/j.msec.2018.06.010.

[14] Utzeri VJ, Ribani A, Bovo S, Taurisano V, Calassanzio M, Baldo D, *et al*. Microscopic ossicle analyses and the complete mitochondrial genome sequence of Holothuria (Roweothuria) polii (Echinodermata; Holothuroidea) provide new information to support the phylogenetic positioning of this sea cucumber species. Marine Genomics. 2020; 51: 100735. https://doi.org/10.1016/j.margen.2019.100735.

[15] Stricker SA. The fine structure and development of calcified skeletal elements in the body wall of holothurian echinoderms. Journal of Morphology. 1986; 188: 273–288. https://doi.org/10.1002/jmor.1051880303.

[16] Tiago CG, Brites AD, Kawauchi GY. A simple enzymatic method for examining calcite ossicles of Echinodermata. Journal of Microscopy. 2005; 218: 240–246. https://doi.org/10.1111/j.1365-2818.2005.01486.x.

[17] Kerr AM. Holothuria (Semperothuria) roseomaculata n. sp. (Aspidochirotida: Holothuriidae), a coral-reef inhabiting sea cucumber from the western Pacific Ocean. Zootaxa. 2013; 3641: 384–394. https://doi.org/10.11646/zootaxa.3641.4.5.

[18] De Carvalho B, Dory E, Trus C, Pirson J, Germain L, Lecloux G, *et al*. Biological performance of a novel bovine hydroxyapatite in a guided bone regeneration model: a preclinical study in a mandibular defect in dogs. Clinical Implant Dentistry and Related Research. 2024; 26: 183–196. https://doi.org/10.1111/cid.13260.

[19] Irastorza-Lorenzo A, Sánchez-Porras D, Ortiz-Arrabal O, de Frutos MJ, Esteban E, Fernández J, *et al*. Evaluation of Marine Agarose Biomaterials for Tissue Engineering Applications. International Journal of Molecular Sciences. 2021; 22: 1923. https://doi.org/10.3390/ijms22041923.

[20] Ortiz-Arrabal O, Bermejo-Casares F, Garzón I, Mesa-García M, Gómez-Llorente C, Alaminos M. Optimization of human skin keratinocyte culture protocols using bioactive molecules derived from olive oil. Biomedicine & Pharmacotherapy = Biomédecine & Pharmacothérapie. 2023; 164: 115000. https://doi.org/10.1016/j.biopha.2023.115000.

[21] Ortiz-Arrabal O, Chato-Astrain J, Crespo PV, Garzón I, Mesa-García MD, Alaminos M, *et al*. Biological Effects of Maslinic Acid on Human Epithelial Cells Used in Tissue Engineering. Frontiers in Bioengineering and Biotechnology. 2022; 10: 876734. https://doi.org/10.3389/fbioe.2022.876734.

[22] Al-Maawi S, Orlowska A, Sader R, James Kirkpatrick C, Ghanaati S. *In vivo* cellular reactions to different biomaterials—Physiological and pathological aspects and their consequences. Seminars in Immunology. 2017; 29: 49–61. https://doi.org/10.1016/j.smim.2017.06.001.

[23] Awadeen MA, Al-Belasy FA, Ameen LE, Helal ME, Grawish ME. Early therapeutic effect of platelet-rich fibrin combined with allogeneic bone marrow-derived stem cells on rats' critical-sized mandibular defects. World Journal of Stem Cells. 2020; 12: 55–69. https://doi.org/10.4252/wjsc.v12.i1.55.

[24] Bumalee D, Lapthanasupkul P, Songkampol K, Srimaneekarn N, Kitkumthorn N, Arayapisit T. Qualitative Histological Evaluation of Various Decalcifying Agents on Human Dental Tissue. European Journal of Dentistry. 2023; 17: 818–822. https://doi.org/10.1055/s-0042-1755615.

[25] Bergholt NL, Lysdahl H, Lind M, Foldager CB. A Standardized Method of Applying Toluidine Blue Metachromatic Staining for Assessment of Chondrogenesis. Cartilage. 2019; 10: 370–374. https:

//doi.org/10.1177/1947603518764262.

[26] Ibáñez-Cortés M, Martín-Piedra MÁ, Blanco-Elices C, García-García ÓD, España-López A, Fernández-Valadés R, *et al*. Histological characterization of the human masticatory oral mucosa. A histochemical and immunohistochemical study. Microscopy Research and Technique. 2023; 86: 1712–1724. https://doi.org/10.1002/jemt.24398.

[27] Carriel VS, Aneiros-Fernandez J, Arias-Santiago S, Garzón IJ, Alaminos M, Campos A. A Novel Histochemical Method for a Simultaneous Staining of Melanin and Collagen Fibers. The Journal of Histochemistry and Cytochemistry: Official Journal of the Histochemistry Society. 2011; 59: 270–277. https://doi.org/10.1369/0022155410398001.

[28] Vela-Romera A, Carriel V, Martín-Piedra MA, Aneiros-Fernández J, Campos F, Chato-Astrain J, *et al*. Characterization of the human ridged and non-ridged skin: a comprehensive histological, histochemical and immunohistochemical analysis. Histochemistry and Cell Biology. 2019; 151: 57–73. https://doi.org/10.1007/s00418-018-1701-x.

[29] Dalfino S, Savadori P, Piazzoni M, Connelly ST, Giannì AB, Del Fabbro M, *et al*. Regeneration of Critical-Sized Mandibular Defects Using 3D-Printed Composite Scaffolds: a Quantitative Evaluation of New Bone Formation in *in Vivo* Studies. Advanced Healthcare Materials. 2023; 12: e2300128. https://doi.org/10.1002/adhm.202300128.

[30] Chen Z, Li Z, Li J, Liu C, Lao C, Fu Y, *et al*. 3D printing of ceramics: a review. Journal of the European Ceramic Society. 2019; 39: 661–687. https://doi.org/10.1016/j.jeurceramsoc.2018.11.013.

[31] Basma HS, Saleh MHA, Geurs NC, Li P, Ravidà A, Wang HL, *et al*. The effect of bone particle size on the histomorphometric and clinical outcomes following lateral ridge augmentation procedures: a randomized double-blinded controlled trial. Journal of Periodontology. 2023; 94: 163–173. https://doi.org/10.1002/JPER.22-0212.

[32] Harini R, Natarajan V, Sunil CK. Sea cucumber significance: Drying techniques and India's comprehensive status. Journal of Food Science. 2024; 89: 3995–4018. https://doi.org/10.1111/1750-3841.17153.

[33] Li M, Gao Y, Qi Y, Song Z, Li Z, Lin Y, *et al*. Assessment of the Nutritional Value of Cultured Sea Cucumber *Apostichopus japonicus*. Journal of Aquatic Food Product Technology. 2021; 30: 868–879. https://doi.org/10.1080/10498850.2021.1949769.

[34] Anderson JM. Future challenges in the *in vitro* and *in vivo* evaluation of biomaterial biocompatibility. Regenerative Biomaterials. 2016; 3: 73–77. https://doi.org/10.1093/rb/rbw001.

[35] Cuende N, Izeta A. Clinical Translation of Stem Cell Therapies: a Bridgeable Gap. Cell Stem Cell. 2010; 6: 508–512. https://doi.org/10.1016/j.stem.2010.05.005.

[36] Rico-Sánchez L, Garzón I, González-Andrades M, Ruíz-García A, Punzano M, Lizana-Moreno A, *et al*. Successful development and clinical translation of a novel anterior lamellar artificial cornea. Journal of Tissue Engineering and Regenerative Medicine. 2019; 13: 2142–2154. https://doi.org/10.1002/term.2951.

[37] Malekpour A, Chen X. Printability and Cell Viability in Extrusion-Based Bioprinting from Experimental, Computational, and Machine Learning Views. Journal of Functional Biomaterials. 2022; 13: 40. https://doi.org/10.3390/jfb13020040.

[38] Martin-Piedra MA, Garzon I, Oliveira AC, Alfonso-Rodriguez CA, Sanchez-Quevedo MC, Campos A, *et al*. Average cell viability levels of human dental pulp stem cells: an accurate combinatorial index for quality control in tissue engineering. Cytotherapy. 2013; 15: 507–518. https://doi.org/10.1016/j.jcyt.2012.11.017.

[39] Tamada H. Three-dimensional ultrastructure analysis of organelles in injured motor neuron. Anatomical Science International. 2023; 98: 360–369. https://doi.org/10.1007/s12565-023-00720-y.

[40] Larouche-Bilodeau C, Cameron CB. Acorn worm ossicle ultrastructure and composition and the origin of the echinoderm skeleton. Royal Society Open Science. 2022; 9: 220773. https://doi.org/10.1098/rsos.220773.

[41] Liu S, Yu JM, Gan YC, Qiu XZ, Gao ZC, Wang H, *et al*. Biomimetic natural biomaterials for tissue engineering and regenerative medicine: new biosynthesis methods, recent advances, and emerging applications. Military Medical Research. 2023; 10: 16. https://doi.org/10.1186/s40779-023-00448-w.

[42] Toker H, Ozdemir H, Ozer H, Eren K. A comparative evaluation of the systemic and local alendronate treatment in synthetic bone graft: a histologic and histomorphometric study in a rat calvarial defect model. Oral Surgery, Oral Medicine, Oral Pathology and Oral Radiology. 2012; 114: S146–S152. https://doi.org/10.1016/j.oooo.2011.09.027.

[43] Ma R, Liu Q, Zhou L, Wang L. High porosity 3D printed titanium mesh allows better bone regeneration. BMC Oral Health. 2023; 23: 6. https://doi.org/10.1186/s12903-023-02717-5.

[44] Lamoureux F, Baud'huin M, Duplomb L, Heymann D, Rédini F. Proteoglycans: key partners in bone cell biology. BioEssays: News and Reviews in Molecular, Cellular and Developmental Biology. 2007; 29: 758–771. https://doi.org/10.1002/bies.20612.

[45] Tera T de M, Nascimento RD, Prado RF do, Santamaria MP, Jardini MAN. Immunolocalization of markers for bone formation during guided bone regeneration in osteopenic rats. Journal of Applied Oral Science: Revista FOB. 2014; 22: 541–553. https://doi.org/10.1590/1678-775720140190.

[46] Hohenester E, Maurer P, Timpl R. Crystal structure of a pair of follistatin-like and EF-hand calcium-binding domains in BM-40. The EMBO Journal. 1997; 16: 3778–3786. https://doi.org/10.1093/emboj/16.13.3778.

[47] Licini C, Vitale-Brovarone C, Mattioli-Belmonte M. Collagen and non-collagenous proteins molecular crosstalk in the pathophysiology of osteoporosis. Cytokine & Growth Factor Reviews. 2019; 49: 59–69. https://doi.org/10.1016/j.cytogfr.2019.09.001.

[48] Camacho D, Jesus JP, Palma AM, Martins SA, Afonso A, Peixoto ML, *et al*. SPARC-p53: the double agents of cancer. Advances in Cancer Research. 2020; 148: 171–199. https://doi.org/10.1016/bs.acr.2020.05.004.

[49] Cairns JR, Price PA. Direct demonstration that the vitamin k-dependent bone gla protein is incompletely γ-carboxylated in humans. Journal of Bone and Mineral Research: The Official Journal of the American Society for Bone and Mineral Research. 1994; 9: 1989–1997. https://doi.org/10.1002/jbmr.5650091220.

[50] Keykhosravani M, Doherty-Kirby A, Zhang C, Brewer D, Goldberg HA, Hunter GK, *et al*. Comprehensive Identification of Post-translational Modifications of Rat Bone Osteopontin by Mass Spectrometry. Biochemistry. 2005; 44: 6990–7003. https://doi.org/10.1021/bi050109p.

[51] Luukkonen J, Hilli M, Nakamura M, Ritamo I, Valmu L, Kauppinen K, *et al*. Osteoclasts secrete osteopontin into resorption lacunae during bone resorption. Histochemistry and Cell Biology. 2019; 151: 475–487. https://doi.org/10.1007/s00418-019-01770-y.

[52] Tarquini C, Mattera R, Mastrangeli F, Agostinelli S, Ferlosio A, Bei R, *et al*. Comparison of tissue transglutaminase 2 and bone biological markers osteocalcin, osteopontin and sclerostin expression in human osteoporosis and osteoarthritis. Amino Acids. 2017; 49: 683–693. https://doi.org/10.1007/s00726-016-2290-4.

[53] Liceras-Liceras E, Garzón I, España-López A, Oliveira AC, García-Gómez M, Martín-Piedra MÁ, *et al*. Generation of a bioengineered autologous bone substitute for palate repair: an *in vivo* study in laboratory animals. Journal of Tissue Engineering and Regenerative Medicine. 2017; 11: 1907–1914. https://doi.org/10.1002/term.2088.

Editor's note: The Scientific Editor responsible for this paper was Chris Evans.

Received: 10th July 2024; **Accepted**: 29th August 2024; **Published**: 14th February 2025